9-1-1981

Theoretical Study of the Structural Phase Transition in $RbCaF_3$

L. L. Boyer
Naval Research Laboratory, Washington, D. C.

John R. Hardy
University of Nebraska - Lincoln

Theoretical study of the structural phase transition in $RbCaF_3$

L. L. Boyer
Naval Research Laboratory, Washington, D. C. 20375

J. R. Hardy
Department of Physics, University of Nebraska, Lincoln, Nebraska 68588

(Received 18 May 1981)

We have made a first-principles study of the structural phase transition at $T_c = 193$ K in $RbCaF_3$, using interionic potentials derived by the Gordon-Kim approach, and a new extension of the quasiharmonic approximation for the free energy. The transition is caused by instability of a triply degenerate R-point vibration which leads to a coordinated rotation of the CaF_6 octahedra. We find that, as the lattice contracts, the quasiharmonic frequency of the R-point vibrations becomes imaginary at approximately 1280 K: Below this temperature the *static* lattice energy, as a function of CaF_6 rotation, has a double minimum. However, the quasiharmonic *free energy* has no minimum for finite rotations until $T \lesssim 125$ K. Thus the present theory predicts that $T_c \cong 125$ K (cf $T_c = 193$ K, experimental). In the region between 125 and about 1280 K "nests" of modes about the zone edges have imaginary quasiharmonic frequencies. By a simple extension of the quasiharmonic theory their contribution to the free energy has also been included. We also predict that the melting temperature is approximately 1350 K, which agrees very well with the measured value of 1382 K. However, the predicted thermal expansion of the perovskite phase at room temperature is $\sim 17\%$ *lower* than the observed value. This leads us to argue that the good agreement between theoretical and experimental melting temperatures is, in part, due to a cancellation between neglected anharmonic effects and certain deficiencies in the interionic potentials. We also find that, for the tetragonal phase, the calculated c/a ratio and rotation angle for the CaF_6 octahedra which minimize the static energy are in good agreement with measured values at low temperature. We also discuss certain more general implications of the present work. Specifically, we suggest that our results indicate that it may be more natural to regard the structural phase transition as arising from the "unfreezing" of the distortion associated with the lower-symmetry phase. Our results also provide a natural explanation for the apparently universal tendency of transition temperatures for zone-boundary instabilities to be raised by hydrostatic stress.

I. INTRODUCTION

One of the most extensively studied structural phase transitions is that which occurs in strontium titanate ($SrTiO_3$) at 110 K, produced by the instability of a triply degenerate vibration at the zone corner or R point. However, none of the theoretical work has attempted to address seriously what appear to us to be, in many respects, the two most fundamental questions: Why does this transition occur, and why does it occur at 110 K? A serious answer to both these (interrelated) questions can only be provided by a theory which involves no disposable parameters. It cannot be provided by phenomenological approaches involving models whose parameters are determined by fitting experimental data: e.g., lattice-dynamical models whose parameters are determined by fitting the measured dispersion curves.

The ideal answer to these questions would be provided by a calculation which derives the free energy from a first-principles quantum-mechanical calculation and predicts that the distorted structure has a lower free energy below 110 K. Such a formidable undertaking has not been attempted for two main reasons: (a) The difficulty of allowing for anharmonic effects in the free energy, and (b) the inability to derive from first principles a reliable potential energy function for the lattice. At present, the second problem presents major difficulties for $SrTiO_3$. However, relatively recent experimental studies[1–6] have revealed that the fluoperovskite, rubidium calcium trifluoride ($RbCaF_3$), shows the same type of lattice instability at 193 K. Also, very recently, it has been found that another isomorph, potassium calcium trifluoride ($KCaF_3$), shows two structural instabilities, one of 560 K and the other at 551 K,[7] both intimately related to zone-boundary lattice instabilities. For these systems calculations are possible, and the purpose of this paper is to present first principles calculations of the equation of state for $RbCaF_3$, which is

the simpler of the two in its behavior.

The present work represents a major extension to more complex systems and instabilities of an approach that was previously used to explain melting of sodium-chloride-structure alkali halides[8,9] and subsequently extended to explain the onset of superionic conductivity in fluorite (CaF_2).[10] This approach has two essential elements: the construction of parameter-free interionic potentials using the Gordon-Kim[11] technique, and the treatment of anharmonic effects using the quasiharmonic approximation. In order to employ the Gordon-Kim approach it is necessary to have accurate knowledge of the free-ion wave functions. This is available for ions such as Rb^+, Ca^{2+}, and F^-, but not for O^{2-}, which is unstable in the free state. Given this knowledge, one assumes that the crystalline charge density is given by a superposition of the constituent free-ion charge densities. The effective interionic potential is then computed from the resultant charge density by treating it as though it is (locally) a free electron gas. In the present work we assume that it is adequate to consider only pairwise overlap: Thus we assume that regions in which three, or more, ions overlap significantly are either negligibly small or nonexistent. We thus obtain a lattice energy that is the sum of pairwise interactions: long-range monopole-monopole interactions, that represent exactly the interaction of the spherical free-ion charge distributions, and short-range interactions between close neighbors that include all the corrections due to ionic overlap. This energy expression is valid for any lattice configuration if we maintain the basic Gordon-Kim premise that the ionic charge distributions are unaffected by their incorporation into a solid. It thus follows that not merely the static lattice energy, but also the free energy is completely determined. This is the case because the dependence of the lattice energy on all degrees of freedom is known exactly, hence all allowed eigenstates of the lattice Hamiltonian are determined, and the system's free energy is, in principle, known exactly. In practice the actual determination of this quantity presents major theoretical problems and approximations are necessary. The simplest, which was employed previously,[8-10] is the quasiharmonic approximation. In this approximation the free energy is written as

$$F(x,T)=U(x)+\tfrac{1}{2}\sum_i h\nu_i(x) + kT\sum_i \ln\left[1-\exp\left(-\frac{h\nu_i(x)}{kT}\right)\right], \quad (1)$$

where h and k are the Planck and Boltzmann constants, respectively, and x represents a set of structural parameters (e.g., volume) on which the static lattice energy, U, and the frequencies, ν_i, depend. These frequencies are those of small amplitude oscillations about the lattice configuration specified by the parameters x. The equilibrium values of these parameters at any given temperature are those which minimize the free energy. Within this quasiharmonic approximation the dependence of F on x is treated exactly. Moreover, as we shall see later, it is possible to go beyond the quasiharmonic approximation when the quasiharmonic frequencies become imaginary.

The equilibrium values of x are determined from the equation of state

$$P_x=-\left(\frac{\partial F}{\partial x}\right)_T, \quad (2)$$

where P_x is the thermodynamic "force" conjugate to the variable x: e.g., if x is the volume, then P_x is the external pressure. However, in the present paper, where we are concerned with the zone-corner instability in $RbCaF_3$, we shall be using Eq. (2) in a more general form. Specifically, we have to allow for the dependence of F on three parameters in the low-temperature phase: the volume, the tetragonal distortion, and the amplitude of the "frozen-in" zone-corner distortion. The forces conjugate to the first two of these present no conceptual problems: That conjugate to the third is a little more difficult to conceive. It is, in fact, a "staggered" force which alternates in sign for different atomic sites. The reason for this is that the R-point instability corresponds to correlated small rotations of all the CaF_6 octahedra, and, to produce such rotations, there must be a torque about the appropriate axis for each octahedron. Experimentally such a "force" would be difficult, if not impossible, to apply but it is a perfectly valid thermodynamic concept and closely analogous to the corresponding "field" in the theory of antiferromagnetism. Under normal conditions P_x will be zero and the equation of state, and thus the equilibrium values of x, x_0, will be determined by the requirements that $(\partial F/\partial x)_{T,x=x_0}=0$ for all x.

In the remainder of this paper we will be describing our theoretical studies in detail. However, before commencing this account, it is appropriate to outline the main qualitative features of our results which we regard as extremely important.

What we find is that above ~125 K the cubic (perovskite) structure is the thermodynamically stable phase. However, below ~1280 K the quasiharmonic frequencies at the R point become imaginary *due to the thermal contraction of the lattice.* We shall elucidate this further later, but the crucial point is that, below a critical volume, the CaF_6 octahedra are in metastable equilibrium at the perovskite sites and can, by coordinated rotation, move to one or other of two adjacent lower minima in the potential energy surface. However, it is not until the tempera-

ture drops below ~125 K that the quasiharmonic free energy has a minimum for a finite *static* value of the amplitude of this coordinated rotation. It is this lower temperature that is the transition temperature: Between 1280 and 125 K the system is executing highly anharmonic motion between the two wells. For the degrees of freedom involved in this motion, special treatment, which we shall describe in due course, is necessary.

Below 125 K the tetragonal structure is not absolutely stable. This is because the soft R-point vibration of the cubic phase is triply degenerate and the distortion stabilizes only one of these three modes: that corresponding to rotations about one specific axis of the CaF_6 octahedron. Statically the lattice would prefer to distort further by some combination of rotations about the other two axes (as appears to happen in $KCaF_3$). However, this lower symmetry phase may not be thermodynamically stable, at least within the quasiharmonic approximation. This belief is based on the wide temperature difference between the point at which the cubic phase becomes *mechanically* unstable and the point where the tetragonal phase becomes *thermodynamically* stable. More specifically, in the limit $T \to 0$, the "phonon pressure," due to the zero-point motion, may be sufficient to disrupt the lower symmetry structure. Experimental results[1,6,12,13] do reveal the existence of a further transition at ~44 K, but the structure of the resultant low-temperature phase seems to be unclear at present: It may be that the phonon pressure due to zero point motion leads to the structure of this phase being other than that which minimizes the static lattice energy. The most definitive work[6] indicates that the 44 K transition involves equal rotations about all three axes of the CaF_6 octahedra. However, it is a markedly first-order transition with large thermal hysteresis. This appears to indicate the presence of a significant barrier in the free-energy surface between the tetragonal phase and this lower symmetry phase.

Finally, it is of interest to observe that the more complex behavior of $KCaF_3$ involves simultaneous rotations of the CaF_6 octahedron about two principle axes at the upper transition and all three axes at the lower transition. Whether it would be possible to explain this behavior using our present approach is an open question. It would certainly present a much more complicated problem, since one would need to include additional x parameters and the calculations would be correspondingly more complex. It seems to us likely, indeed probable, that the present theory would predict at least one transition to a lower symmetry structure. However, what this structure would be is unclear. Moreover, whether two successive transitions would be predicted is much less certain.

We shall now proceed to a detailed discussion of the various stages of our calculations.

II. STATIC LATTICE ENERGY

In order to study the relative static stability of the low-temperature tetragonal phase versus that of the ideal perovskite structure, it is necessary to compute the static energy of the lower symmetry phase as a function of both volume *and* the parameters that specify the distortion from the higher symmetry structure. These variables together constitute the x parameters. This study is necessary in order to understand the interplay between all these parameters, and the physical origins of the lattice distortion. Once we have such an understanding it is then possible to proceed to a study of the free energy and its minimization with respect to the x parameters. While it would, in principle, be possible to proceed directly to this minimization, in practice such computations are very time consuming, and one thus wishes to reduce the number of variables to be considered as much as possible. A definitive knowledge of the potential surfaces in the hyperspace of x parameters is a great help in this respect, and can be obtained relatively rapidly.

In Fig. 1 we show four unit cells of the perovskite structure which together define the primitive unit cell of the low-temperature phase. The open circles denote Rb^+ ions and the four octahedra, with large solid circles at their centers and small solid circles at their corners, give the positions of the Ca^{2+} and F^- ions, respectively. The arrows indicate the low-

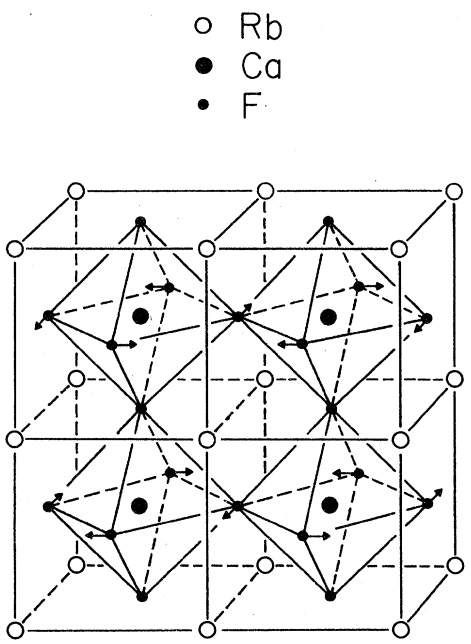

FIG. 1. Four unit cells of the perovskite structure with arrows at corners of the CaF_6 octahedra indicating the distortion produced by the transition to the low-temperature phase.

temperature distortion. In Table I we list the coordinates of the 20 ions in the unit cell of the low-temperature structure. The components in the x and y directions are in units of $\sqrt{2}a$, where a is the cube cell side of the perovskite structure. Along the z direction the components are in units of $2c$, where $c=a$ in the perovskite structure.

For the x parameters which specify the low-temperature structure it is convenient to take $b=(a^2c)^{1/3}$, $f=c/a$, and $\delta=u-\frac{1}{4}$. If $f=1$ and $\delta=0$ then we have the perovskite structure with $a=b=c$. The distortion from the perovskite structure when $\delta\neq 0$ corresponds approximately to a cooperative rotation of the CaF_6 octahedra through angles of $\pm 4\delta$.

The distinct bonds that we found necessary to consider for accurate computation of the short-range component of the energy in the low-temperature phase are listed below. In each case the bond length r_i is given together with the number of bonds n_i having that length:

Nearest-neighbor Ca–F

$$r_1=(\tfrac{1}{16}+\delta^2)^{1/2}2a,\quad n_1=16\ , \tag{2a}$$

$$r_2=\frac{fa}{2},\quad n_2=8\ . \tag{2b}$$

Nearest-neighbor Rb–F

$$r_3=\frac{a}{\sqrt{2}},\quad n_3=16\ , \tag{3a}$$

$$r_4=[4(\tfrac{1}{4}+\delta)^2+\tfrac{1}{4}f^2]^{1/2}a,\quad n_4=16\ , \tag{3b}$$

$$r_5=[4(\tfrac{1}{4}-\delta)^2+\tfrac{1}{4}f^2]^{1/2}a,\quad n_5=16\ . \tag{3c}$$

Nearest-neighbor F–F

$$r_6=(\tfrac{1}{2}+8\delta^2)^{1/2}a,\quad n_6=16\ , \tag{4a}$$

$$r_7=(\tfrac{1}{4}+4\delta^2+\tfrac{1}{4}f^2)^{1/2}a,\quad n_7=32\ . \tag{4b}$$

Second neighbor F–F

$$r_8=fa,\quad n_8=4\ , \tag{5a}$$

$$r_9=a,\quad n_9=8\ , \tag{5b}$$

$$r_{10}=(1+16\delta^2)^{1/2}a,\quad n_{10}=8\ , \tag{5c}$$

$$r_{11}=(1+4\delta)a,\quad n_{11}=4\ , \tag{5d}$$

$$r_{12}=(1-4\delta)a,\quad n_{12}=4\ , \tag{5e}$$

$$r_{13}=(f^2+16\delta^2)^{1/2}a,\quad n_{13}=8\ . \tag{5f}$$

Third neighbor F–F

$$r_{14}=[2(\tfrac{1}{2}+2\delta)^2+f^2]^{1/2}a,\quad n_{14}=16\ , \tag{6a}$$

$$r_{15}=[2(\tfrac{1}{2}-2\delta)^2+f^2]^{1/2}a,\quad n_{15}=16\ , \tag{6b}$$

$$r_{16}=[2(\tfrac{1}{4}+\delta)^2+2(\tfrac{3}{4}+\delta)^2+\tfrac{1}{4}f^2]^{1/2}a,\quad n_{16}=32\ , \tag{6c}$$

$$r_{17}=[2(\tfrac{1}{4}-\delta)^2+2(\tfrac{3}{4}-\delta)^2+\tfrac{1}{4}f^2]^{1/2}a,\quad n_{17}=32\ . \tag{6d}$$

The component of the static lattice energy due to the long-range Coulomb interaction can be written as $\alpha(\delta,f)/b$, where $\alpha(\delta,f)$ is an effective Madelung constant, explicitly dependent on both δ and f. For values of δ and f within the range of interest to our studies, ($|\delta|<0.04, 0.99<f<1.01$)$\alpha$ is given to

TABLE I. Positions of the 20 ions in one unit cell of the low-temperature phase of $RbCaF_3$. The x and y coordinates are in units of $\sqrt{2}\,a$ and z coordinates in units of $2c$. When $c=a$ and $u=\frac{1}{4}$ the structure is perovskite with lattice constant a.

Ion	Coordinates x	y	z
Ca	0	0	0
Ca	0	0	$\frac{1}{2}$
Ca	$\frac{1}{2}$	$\frac{1}{2}$	0
Ca	$\frac{1}{2}$	$\frac{1}{2}$	$\frac{1}{2}$
Rb	$\frac{1}{2}$	0	$\frac{1}{4}$
Rb	$\frac{1}{2}$	0	$\frac{3}{4}$
Rb	0	$\frac{1}{2}$	$\frac{1}{4}$
Rb	0	$\frac{1}{2}$	$\frac{3}{4}$
F	0	0	$\frac{1}{4}$
F	0	0	$\frac{3}{4}$
F	$\frac{1}{2}$	$\frac{1}{2}$	$\frac{1}{4}$
F	$\frac{1}{2}$	$\frac{1}{2}$	$\frac{3}{4}$
F	u	$u-\frac{1}{2}$	0
F	$-u$	$\frac{1}{2}-u$	0
F	$u-\frac{1}{2}$	$-u$	0
F	$\frac{1}{2}-u$	u	0
F	$u-\frac{1}{2}$	u	$\frac{1}{2}$
F	$\frac{1}{2}-u$	$-u$	$\frac{1}{2}$
F	u	$\frac{1}{2}-u$	$\frac{1}{2}$
F	$-u$	$u-\frac{1}{2}$	$\frac{1}{2}$

TABLE II. Values obtained for c and β by fitting the exponential form, $ce^{-\beta r}$, to calculated values of the short-range Coulomb (SRC), kinetic (KE), exchange (ex), and correlation (corr) contributions to the indicated pair potentials in the range r_l to r_u. Results are in atomic units with energy in hartree.

Ion pair	c, β	SRC	KE	ex	corr	r_l	r_u
CaF	c	−34.937 0	98.648 8	−10.271 4	−0.224 891	3.8	4.6
CaF	β	1.910 88	1.780 84	1.479 84	1.111 59	3.8	4.6
RbF	c	−45.683 3	96.569 3	−10.221 4	−0.288 258	5.6	6.0
RbF	β	1.707 20	1.597 77	1.305 91	1.005 48	5.6	6.0
FF	c	−17.738 7	25.105 5	−2.980 54	−0.117 815	5.4	6.4
FF	β,	1.556 12	1.403 05	1.107 56	0.846 702	5.4	6.4

seven-place accuracy by

$$\alpha(\delta,f) = -49.509\,872 + 111.218\delta^2 + 1326.38\delta^4 - 617.89\delta^2(1-f) + 5490\delta^4(1-f) - 13.65(1-f)^2 - 462\delta^2(1-f)^2 - 60\,000\delta^4(1-f)^2 \quad . \tag{7}$$

On combining both parts (Coulomb and short-range) of the static lattice energy one obtains the energy per unit cell of the low-temperature phase:

$$U(b,\delta,f) = \frac{\alpha(\delta,f)}{b} + \Phi_{\mathrm{CaF}} + \Phi_{\mathrm{RbF}} + \Phi_{\mathrm{FF}} \quad , \tag{8a}$$

where

$$\Phi_{\mathrm{CaF}} = \sum_{i=1}^{2} n_i \phi_{\mathrm{CaF}}(r_i) \quad , \tag{8b}$$

$$\Phi_{\mathrm{RbF}} = \sum_{i=3}^{5} n_i \phi_{\mathrm{RbF}}(r_i) \quad , \tag{8c}$$

$$\Phi_{\mathrm{FF}} = \sum_{i=6}^{17} n_i \phi_{\mathrm{FF}}(r_i) \quad , \tag{8d}$$

and the $\phi(r)$'s represent the short-range parts of the various potentials. For each interaction these were determined for several values of r within the range of interest using Green and Gordon's program POTLSURF.[14] Each contribution to a given potential [electrostatic (SRC), kinetic (KE), exchange (ex), and correlation (corr)] varies approximately exponentially with r over this range and it was thus possible to "best-fit" exponentials to each separate contribution. The value of c and β in the exponential form $ce^{-\beta r}$, determined by fitting to results from program POTLSURF at several r values in the range of separations of interest here (r_l to r_u) are shown in Table II. These values differ somewhat from those published earlier[8,10] due to the use of different ranges of separations in the fitting procedure. Within the range r_l to r_u the fitted potentials agree with the true ones to better than 0.2%. Slight modifications of this procedure were tested to be sure they produced only minor quantitative changes in our results. The values in Table II are given to six decimals to enable the reader to make a precise comparison with our results.

Using these fitted potentials it was then possible to find the values of b, f, and δ (b_0, f_0, δ_0) which minimize the total static energy. The results are shown in Table III for several models which

TABLE III. Comparison of the structure parameters (b_0, f_0, and δ_0), which minimize the static energy (U) of the low-temperature phase of $RbCaF_3$ and the double-well depth [$U(b_0,1,0) - U(b_0,f_0,\delta_0)$] for various models which differ in the number of neighboring ions included in the sum over the short-range interactions.

Model number	Number of shells[a] CaF	RbF	FF	Structure parameters that minimize U b_0 (bohr)	f_0	δ_0	Energy (hartree) $U(b_0,f_0,\delta_0)$	$U(b_0,1,0) - U(b_0,f_0,\delta_0)$
1	1	1	1	8.257 634	1.006 316	0.028 833 7	−5.390 779	0.000 831
2	1	1	2	8.244 963	1.007 708	0.031 344 0	−5.399 708	0.001 206
3	1	1	3	8.234 084	1.009 027	0.033 789 1	−5.404 778	0.001 631
4	2	1	3	8.230 914	1.009 387	0.034 275 2	−5.406 168	0.001 724
5	1	2	3	8.229 262	1.009 286	0.034 156 5	−5.406 984	0.001 705
6	1	1	4	8.232 220	1.009 105	0.033 891 1	−5.405 632	0.001 651
7[b]	1	1	3	8.245 002	1.007 804	0.031 226 2	−5.399 675	0.001 173

[a]A shell is defined in the perovskite structure ($f=1$, $\delta=0$). [b]Same as 3 but with CaF_6 rotations in phase along the z direction.

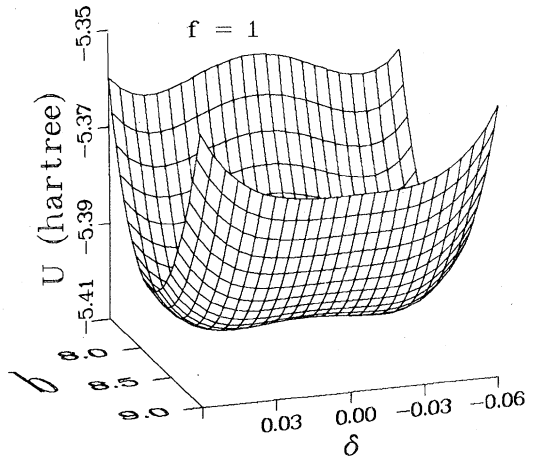

FIG. 2. Potential energy surface as a function of b and δ with $f=1$.

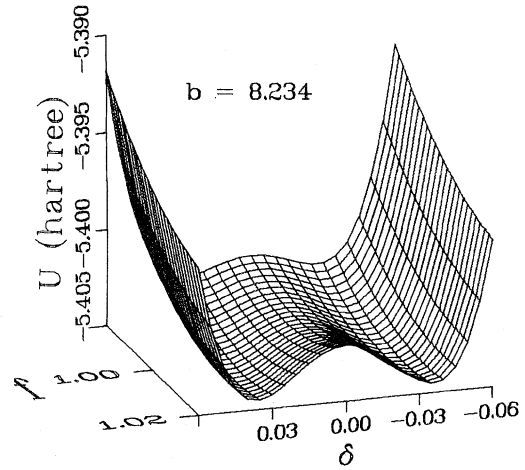

FIG. 3. Potential energy surface as a function of δ and f with $b=8.23$ bohr.

differ in the numbers of shells for which the short-range forces are included: "Shell," in this context refers to a shell of neighbors in the perovskite structure. Also shown in Table III are the absolute minimum static energy $U(b_0,f_0,\delta_0)$, obtained by solving $\partial U/\partial b=\partial U/\partial f=\partial U/\partial\delta=0$, and the difference between $U(b_0,1,0)$ and $U(b_0,f_0,\delta_0)$ which measures the depths of the two minima corresponding to $\pm\delta_0$. It can be seen that the results of model 3 and those which include more distant neighbors are very close, demonstrating that the summations in model 3 are essentially converged. Thus model 3 was used in all subsequent calculations and it is this model to which Eqs. (2)–(8) refer. Models 1 and 2 can be obtained by eliminating terms from the short-range part of U: models 4–6 involve adding additional terms whose explicit form is not worth reproducing as we make no further use of them. Short-range interactions between cations are completely negligible.

The values obtained for b_0, f_0, and the rotation angle $\theta_0\cong 4\delta_0$, are close to the experimental values at low temperature (see below). However, direct comparisons should be treated with caution since the experimental results are strictly only comparable with results obtained by minimizing the *free energy*. What is much more important, at this stage, is an exploration of the potential energy hypersurface. To this end we show the following: (a) in Figs. 2 and 3, three-dimension plots of U vs b and δ and f and δ, respectively; (b) in Fig. 4, U vs δ is plotted for a sequence of b values with $f=1$; and (c) in Fig. 5 U vs

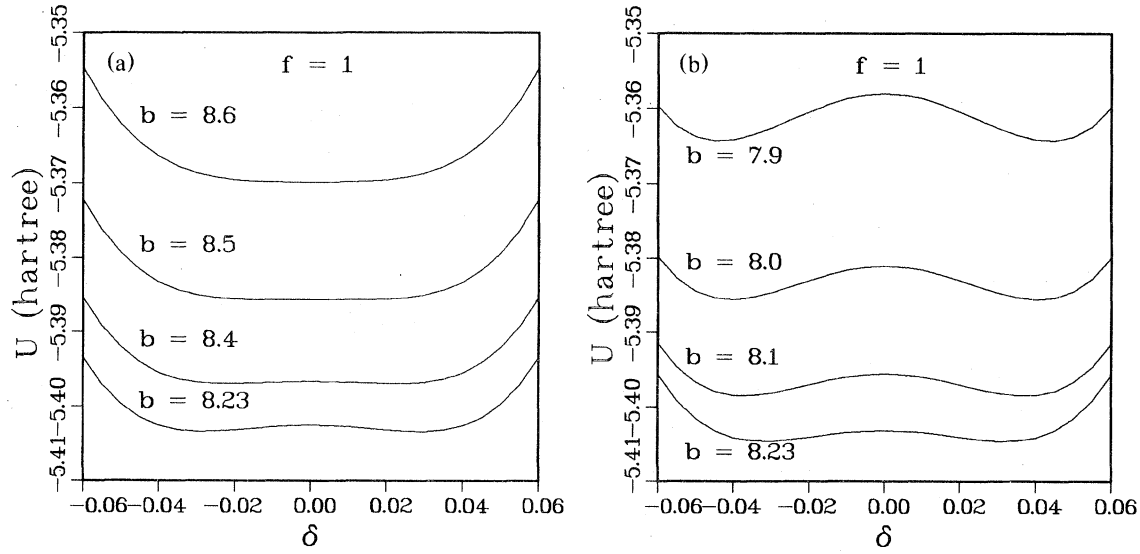

FIG. 4. (a) Potential energy as a function of δ for selected b's ($b>8.23$ bohr) with $f=1$. (b) Potential energy as a function of δ for selected b's ($b<8.23$ bohr) with $f=1$.

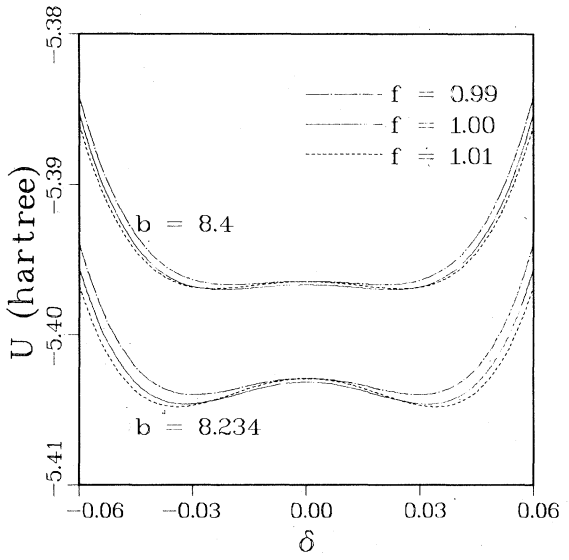

FIG. 5. Potential energy as a function of δ for various selected values of b and f.

δ is plotted for a sequence of f values with $b = 8.234$ and 8.4. Finally, in Fig. 6, we show the various individual contributions to U: the Coulomb part, and the short-range components; shown separately for first-neighbor calcium-fluorine interactions, first-neighbor rubidium-fluorine interactions, and for all the fluorine-fluorine interactions considered in model 3. The plots in Fig. 6 show the four terms in Eq. (8a) as a function of δ for selected b's, using equal energy scales for each plot to facilitate the comparison of their relative strengths.

From these plots we can draw a number of specific conclusions.

(a) Figures 2–5 reveal that the dependence of U on f is relatively insignificant compared to its dependence on b and δ.

(b) Figures 2 and 4 show clearly that, as the lattice contracts, a double minimum develops in U as a function of δ when $b \leq 8.555$ (bohr). This signifies that certain of the quasiharmonic normal-mode frequencies for the perovskite structure become imaginary when the crystal volume shrinks below $(8.555)^3$ (bohr).[3] However, as we shall see later, this does *not* signify an immediate transition to the low-temperature structure.

(c) Figure 6 demonstrates that the basic cause of the static instability of the perovskite structure is a competition between the short-range part of the Ca-F interactions and that of the Rb-F interactions. Both the total Coulomb potential and Rb-F short-range interactions tend to maintain the perovskite structure, but the short-range Ca-F interactions are always reduced by a finite value of δ. Thus, as b is reduced, there comes a point when the Ca-F interactions dominate and produce the CaF_6 rotations. However, this causes r_5 for the Rb-F bonds to decrease and the rotation is stabilized at some finite value of δ. On the other hand, Fig. 6(d) indicates that the F-F interactions are nearly independent of δ: However, they do have quantitative effects on the magnitude of the rotation and the depth of the double well, as can be seen from the results in Table III. This results from the fact that Φ_{FF} is negative, which lowers the equilibrium value of b, causing the double well to deepen. However, from Fig. 7, we see that the double-well structure in the potential surface is still present, even when the F-F short-range interactions are completely omitted.

The present calculation is for one specific material, but it appears highly plausible to argue that the presence or absence of a zone-boundary instability of the present type in *any* AMX_3 system is likely to be determined by the type of balance between M-X and A-X short-range forces that we have found in $RbCaF_3$. Thus, as the "size" of the A ions increases relative to that of the M ions, the perovskite phase will be stabilized. This concept is very close to the semiempirical approach of Rousseau *et al.*[2] based on the idea of close packing of hard spherical ions showing characteristic radii. The difference is that our general prediction stems from a first principles calculation of the potential for a given AMX_3 structure. This calculation is, to the best of our knowledge, the first of its kind for such a system.

At this point a note of caution should be introduced regarding predictions as to the low-temperature structure. We have studied the static lattice energy of a particular low-temperature phase in which the CaF_6 octahedra are allowed to rotate about the one axis only. However, like the perovskite structure, this too is statically metastable since the unstable R-point vibrations of the perovskite phase are triply degenerate and only one of these vibrations is stabilized by rotations about a single axis: the other two remain unstable. Thus the absolute minimum of U presumably corresponds to some superposition of rotations about all three axes. This will presumably hold true for any AMX_3 system for which the perovskite structure is metastable. However, there is little point in searching for this absolute minimum, at least for $RbCaF_3$, since the actual structure is that which minimizes the free energy. Thus, once the first instability has developed, as the structure is cooled, its subsequent transitions (if any) will result from a change in the balance between competing contributions to its free energy. Here we have made the implicit assumption that, for $RbCaF_3$, the primary energy decrease is due the CaF_6 octahedra rotations about the single preferred axis: The other two possible rotations are assumed to have only secondary effects. If this is the case, the free energy surface will follow the potential surface at the first transition. Subsequently this may well not be the case. In other

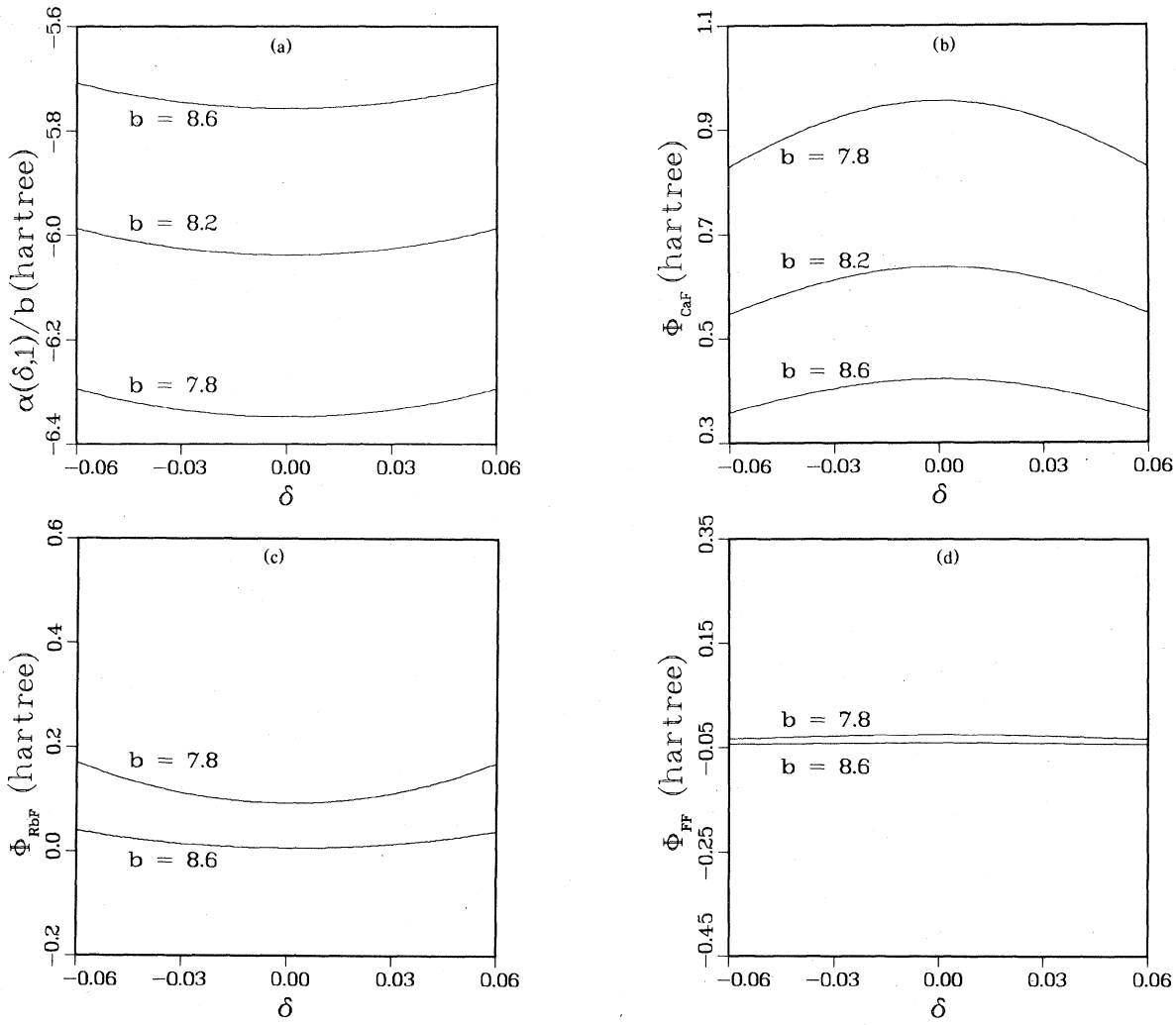

FIG. 6. Separate contributions to the δ dependence of the potential energy for selected values of b, from (a) the long-range Coulomb interaction, (b) the short-range Ca-F interaction, (c) the short-range Rb-F interaction, and (d) the short-range F-F interaction, plotted on a single-energy scale to facilitate comparison of their relative strengths.

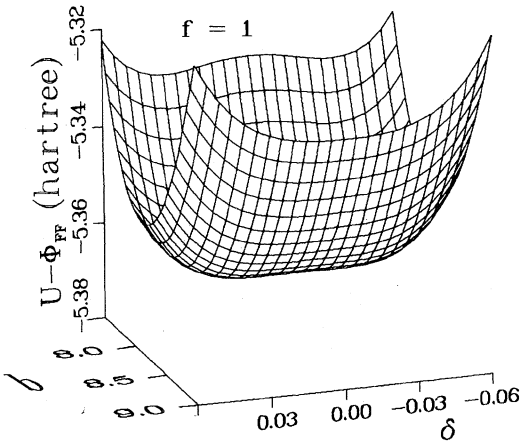

FIG. 7. Potential energy surface for $f=1$ with the short-range part of the F-F interactions excluded.

systems, e.g., $KCaF_3$, the effects of the remaining two rotations may be of primary importance leading to very significant changes in the static energy. In these circumstances we would expect more complex transition behavior and the free-energy surface may not follow the potential-energy surface even at the first transition. Examples of this general type of behavior are provided by "quantum ferroelectrics," which are systems where the distorted ferroelectric phase, although of lower static energy, is never achieved, since it is destabilized by zero-point motion.

III. LATTICE DYNAMICS OF $RbCaF_3$

Before we proceed to an examination of the free energy of $RbCaF_3$ and to predictions of its behavior

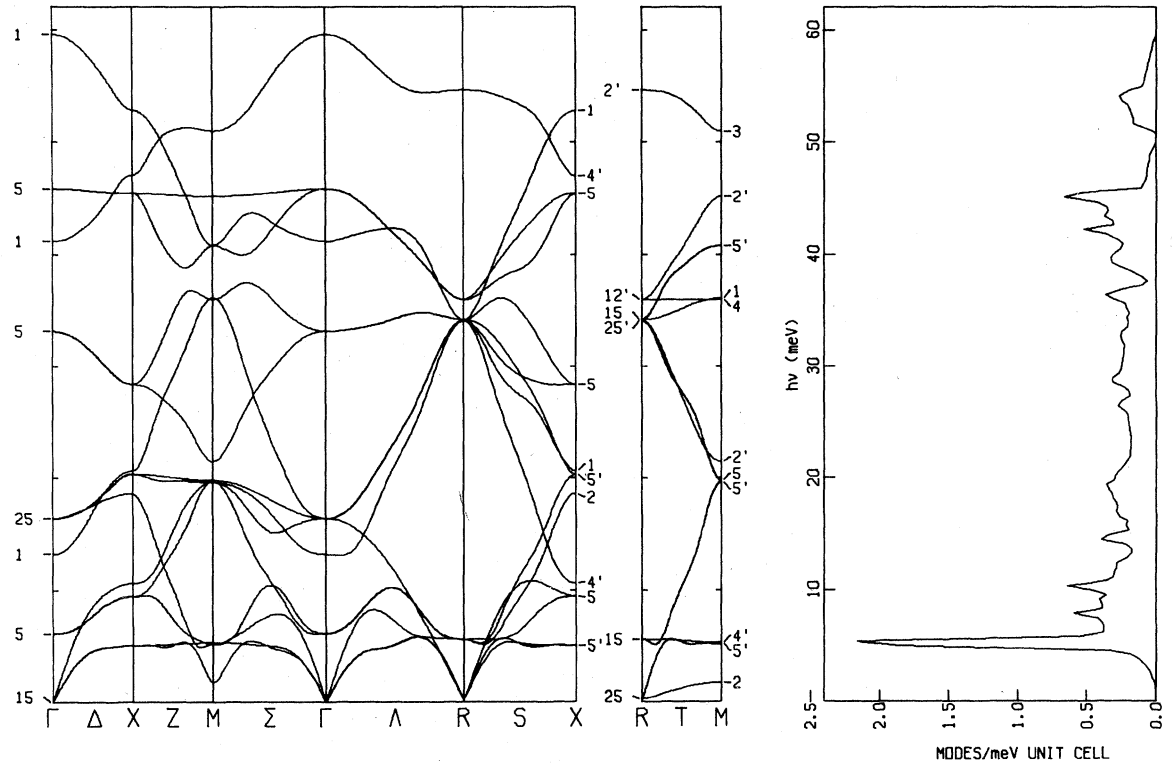

FIG. 8. Quasiharmonic frequency dispersion curves and frequency spectrum for $RbCaF_3$ in the perovskite structure at the critical volume ($b = 8.555$ bohr) below which the R_{25} frequency is imaginary.

using the quasiharmonic approximation, it is important to examine the quasiharmonic frequencies obtained from the dynamical matrix generated from the second derivatives of our potential. It is also important to stress that these "frequencies" are not necessarily comparable with those measured by experimental probes. They are the product of a variational fit to the free energy involving a limited number of parameters; namely, those that define the crystal structure. At this, the simplest level which can provide meaningful results, the frequencies themselves are not variational parameters.

In Fig. 8 we show plots of the dispersion curves and the associated density of states for $RbCaF_3$. These plots have a common energy axis (we chose to plot $h\nu$ rather than ν for reasons of convenience) and have been made for $b = 8.555$ (bohr) which is the critical b below which the double well in U versus δ appears. It can be seen that the energy of the triply degenerate R_{25} modes is essentially zero, signifying that these modes are about to become unstable. The symmetry designations for the various branches were made by comparing their eigenvectors with those published by Cowley[15]; however, the labels have been changed to follow the convention set by Bouckaert *et al.*[16] Differences exist for the Σ, S, M, and X symmetries and these are listed in Table IV.

The phonon dispersion curves were plotted using symmetrized Fourier (SF) interpolation[17] from an $L = 8$ mesh of eact values ($L/2$ is the number of partitions of a given symmetry line). The density of states was computed by applying the tetrahedron

TABLE IV. Relation between the symmetry notation used by Cowley (Ref. 15) and that originally established in Ref. 16 (BSW). Differences exist for Σ, S, M, and X symmetries.

	Σ and S				M and X									
Cowley	1	2	3	4	1	2	3	4	1′	2′	3′	4′	5	5′
BSW	1	2	4	3	1	4	2	3	1′	4′	2′	3′	5	5′

method[18] to an $L=16$ mesh of values obtained by SF interpolation from the $L=8$ mesh. Occasionally, when there is a sharp kink in the dispersion curves, such as that produced when two branches of like symmetry nearly cross, a ripple effect can be seen in the SF interpolated values unless a sufficiently fine mesh is used. This is the case for the two lowest T_5 branches, whose near crossing at about $\frac{1}{4}$ of the distance from R to M produces the slight wiggle seen in the upper of these two branches as M is approached. The third T_5 branch appears to have a similar wiggle, but in this case it is a genuine effect: It does in fact cross the lowest T_2' branch in two places.

The nonzero eigenvector components of the R_{25} modes are given by[15]

$$e_y(F_{\rm I}) = -e_z(F_{\rm II}), \quad \text{mode 1}, \tag{9}$$

$$e_x(F_{\rm I}) = -e_z(F_{\rm III}), \quad \text{mode 2}, \tag{10}$$

$$e_x(F_{\rm II}) = -e_y(F_{\rm III}), \quad \text{mode 3}, \tag{11}$$

where the $F_{\rm I}$, $F_{\rm II}$, and $F_{\rm III}$ ions are at $a(\frac{1}{2},\frac{1}{2},0)$, $a(\frac{1}{2},0,\frac{1}{2})$, and $a(0,\frac{1}{2},\frac{1}{2})$, respectively. The third eigenvector [Eq. (11)] corresponds to CaF_6 rotations about the z axis (see Fig. 1) in the same sense as those associated with a nonzero value of δ. The first and second eigenvector are equivalent, except that they describe rotations about the x and y axes.

It should also be noted that the entire T_2 branch (from R_{25} to M_2) is soft. Moreover, the eigenvectors for the M_2 modes at $\vec{q}=(0,\pi/a,\pi/a)$, $(\pi/a,0,\pi/a)$, and $(\pi/a,\pi/a,0)$ are identical with those for the $R_{25}(1)$ [Eq. (9)], $R_{25}(2)$ [Eq. (10)], and $R_{25}(3)$ [Eq. (11)] modes, respectively. Each of these identities extends also to all modes connecting R_{25} to M_2, namely the T_2 branches, $T_2(1)$, $T_2(2)$, and $T_3(3)$. Physically this means that the only difference between the displacement patterns of the various modes along, and at the ends of, a given T_2 branch is in the relative phase of the CaF_6 octahedra rotations in adjacent planes. For example, the $R_{25}(3)$ mode produces a displacement pattern that reproduces the low-temperature structure (Table I) with $f=1$. In this mode the octahedral rotations are π out of phase in adjacent units parallel to the z axis. On the other hand, the M_2 mode at $\vec{q}=(\pi/a,\pi/a,0)$ [to which $R_{25}(3)$ is connected by the T_2 branch parallel to the z axis of reciprocal space] gives almost the same structure, except that the corresponding rotations about the z axis are all in phase. Between the two extremes the relative phases of these rotations are determined by q_z. Interestingly, if one of these modes were the first to become unstable, the low-temperature phase would have an incommensurate structure. However, this is unlikely for the perfect crystal, since the coupling between rotations about the z axis for octahedra in different planes (perpendicular to that axis) is likely to be dominated by first-neighbor interactions. If this is the case a monotonic variation of frequency with q_z is to be expected.

For a clear insight into the situation in the low-temperature phase it is important to examine the behavior of the three soft T_2 branches of the perovskite phase in the low-temperature structure. In the Brillouin zone of the latter structure the $T_2(3)$ branch starts and ends at the zone center, since it is folded back at $\vec{q}=(0,0,\pi/2c)$. $T_2(1)$ and $T_2(2)$ become equivalent in the low-temperature phase translating into branches that originate at the zone center (the new location of their R_{25} origin) and end at $\vec{q}=(\pi/\sqrt{2}a,\pi/\sqrt{2}a,0)$ and $\vec{q}=(-\pi/\sqrt{2}a,\pi/\sqrt{2}a,0)$.

In Fig. 9 we show the behavior of these three branches as a function of δ for $b=8.234\,084$ (bohr) (the value which minimizes the static energy) and $f=1$. It can be seen that the $T_2(3)$ branch hardens rapidly as δ is increased: This is not the case for the $T_2(1)$ and $T_2(2)$ branches. Specifically, a calculation of the $M_2(1,2)$ frequency, for b, f, and δ all set at the values which minimize the static energy, gives $(h\nu)^2=-0.65$ (meV)^2 for this frequency. Thus a static distortion having the displacement pattern of either mode would further lower the potential energy. However, it may not lower the free energy and may thus not occur. The basic origin of this residual instability is that the tendency of the CaF_6 octahedra to rotate about both x and y axes, in addition to the z axis, is still present in the low-temperature structure. However, it would appear from Fig. 9 that it is signi-

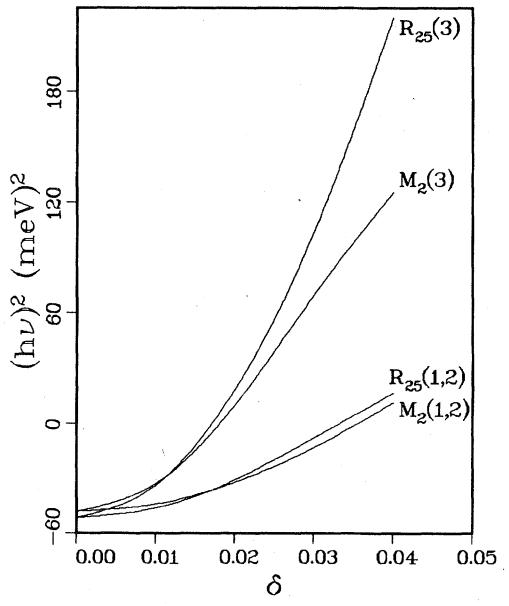

FIG. 9. Plot of the square the "frequencies" of the low-lying R_{25} and M_2 modes as a function of the low-temperature distortion parameter, δ, with $b=b_0$ and $f=1$.

ficantly inhibited by the built-in rotations about the z axis associated with finite δ.

The principal result of these quasiharmonic lattice-dynamical studies is the demonstration of the existence of groups of imaginary frequencies in both the high-temperature phase for $b < 8.555$ (bohr) and in the low-temperature phase. This presents a problem which has to be addressed during the free-energy studies which are the subject of the next section.

IV. FREE-ENERGY CALCULATIONS AND PREDICTION OF THE TRANSITION TEMPERATURE

We are now in a position to examine the occurrence of the phase transition in $RbCaF_3$. We thus, in principle, have to carry out a minimization of the quasiharmonic free energy F, defined by Eq. (1), with respect to all three x parameters (b, f, and $u = 0.25 - \delta$) at a sequence of temperatures. However, the low-temperature structure will only be stable if there exists a minimum in F for $u \neq 0.25$. Otherwise the only minimum in F occurs when $u = 0.25$ and $f = 1$, and we have the perovskite structure as the stable phase: In this phase the only variational parameter is $b = a$ the lattice constant. Since we had already established that the static energy is most strongly dependent on δ we have only made a detailed study of the dependence of F on this parameter and then checked that the predicted transition temperature was relatively insensitive to variations in b and f. In this way we were able to avoid the much more computationally expensive triple minimization.

In Fig. 10 we show the free energy of the low-temperature phase as a function of u, for $b = b_0$ and $f = 1$, at a sequence of temperatures between 0 and 150 K. The problem of the unstable modes associated with the $T_2(1)$ and $T_2(2)$ branches was dealt with by excluding from the sum over modes in F all those unstable for the smallest finite value of $\delta(u = 0.23)$ considered [for $u \gtrsim 0.23$ the $T_2(3)$ branch is unstable in the quasiharmonic approximation]. The justification for this procedure will be given later in our discussion of the perovskite phase. It can be seen that these curves have broad minima away from $u = 0.25$ for $T \lesssim 125$ K: Above this temperature the only minimum is at $u = 0.25$. Thus the present quasiharmonic theory predicts that the transition temperature is between 125 and 150 K. As the $T_2(3)$ branch is unstable for $u \gtrsim 0.23$, we expect the transition to be mildly first order. The predicted transition temperature is *much below* the temperature ($\sim$1280 K) where our studies of the perovskite phase show that the R-point vibrations become unstable, signifying the onset of a double minimum in the *static* energy.

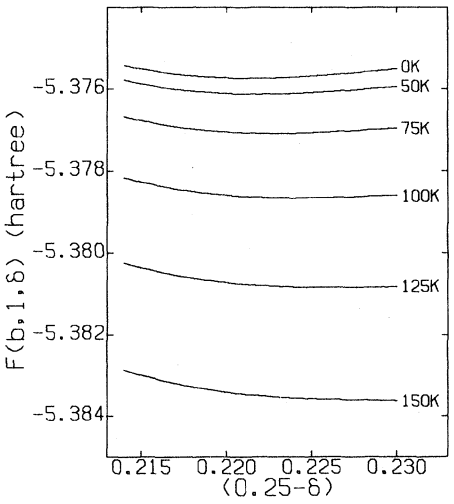

FIG. 10. Free energy of the low-temperature phase as a function of δ at selected temperatures with $b = b_0$ and $f = 1$.

The use of a larger b, to account for thermal expansion, tends to lower the transition temperature by 10–20 K, while the use of $f = f_0$ raises the transition temperature by a similar amount. Thus the transition temperature is not very sensitive to reasonable changes in b and f. The crucial point is that the quasiharmonic theory predicts that *thermodynamic stability* of the low-temperature phase does not occur until the temperature has been reduced by an order of magnitude below the value at which *mechanical instability* develops in the high-temperature structure. Why this should be is best explained by examining the origin of the instability of the low-temperature phase. The key factor here is that the frequency of the $R_{25}(3)$ mode in this phase is strongly dependent on δ. As the temperature is raised, thermal excursions about the static value of δ increase; this tends to decrease δ; the $R_{25}(3)$ frequency is thus reduced, favoring larger thermal fluctuations, and the low-temperature structure thus "bootstraps" itself into instability by reducing δ below the critical value necessary for the frequency of $R_{25}(3)$ to be real. Further, we would argue that the stability of any lower symmetry phase would be determined by similar considerations. In this regard we note that zero-point motion alone may be sufficient to destabilize any further lower symmetry phases, in spite of their potential to lower the static energy.

In the high-temperature perovskite phase, since there is only one variational parameter to be explored, it is relatively inexpensive to obtain the theoretical equation of state and thus to compute the variation of lattice constant with temperature. The only problem is that presented by the unstable quasiharmonic frequencies. We dealt with this in three ways.

(a) We simply omitted from the sum over modes in F all modes for which the frequencies are ima-

ginary at the smallest volume considered ($a = 8.2$ bohr).

(b) We did the same thing but "renormalized" the free energy, i.e., we multiplied the vibrational contribution by $N/(N-n)$, where N is the total number of modes per unit volume and n is the number which have imaginary frequencies at $a = 8.2$ bohr.

(c) We made a classical approximation to the free-energy contribution of the excluded degrees of freedom which goes beyond the quasiharmonic approximation.

The first two approximations are self-explanatory: The third requires elaboration. First we examined the manner in which the static energy U varies with the finite amplitude distortion associated with the M-point instability: This exactly paralleled the static-energy studies of the R-point instability described in Sec. II of the present paper. We found, not too surprisingly, that the two were very similar (see Table III). We thus argued that the dependence on amplitude is the same for *all* the harmonically unstable degrees of freedom. This is based on the fact (see Sec. III) that all these degrees of freedom are basically composed of rotations of the CaF_6 octahedra about the z axis: The only difference between them is in the relative phases of these rotations in adjacent planes. Since the R- and M-point motions, which represent the two extremes in these relative phases, have very similar static energy versus amplitude curves, the same should be true for *all* the unstable modes. Thus we added to the free energy a term

$$F_\delta = nkT \ln \int_{-\infty}^{\infty} \exp\left[\frac{U(b,1,\delta) - U(b,1,0)}{4kT}\right] d\delta \quad . \tag{12}$$

This corresponds to the classical contribution to the potential-energy part of F from these degrees of freedom if we assume that δ now represents the amplitude of *any* of the unstable motions and make the approximation of treating these modes as independent anharmonic oscillators. The factor of $\frac{1}{4}$ in the exponential normalizes U to the perovskite unit cell. Since the classical kinetic-energy contribution to F does not depend on volume, it does not influence the lattice constant and we did not include it.

In Fig. 11 we show curves of the negative of the vibrational pressure and the static pressure versus lattice constant for the perovskite phase of $RbCaF_3$, calculated for a sequence of temperatures: Approximation (3) was used for the unstable modes. The temperature dependence of the lattice constant is given by the intersections of the family of vibrational pressure curves with the static pressure. Thermal expansion data for $RbCaF_3$ show the lattice constant increasing by 0.18% from 200 to 300 K while the theoretical result is 0.15%.

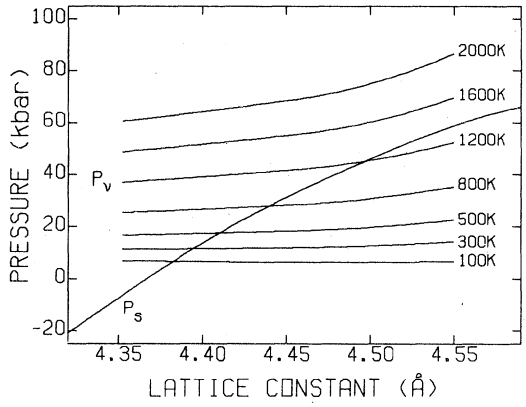

FIG. 11. Vibrational pressure, P_v, at selected temperatures and the static pressure, RP_s as a function of lattice constant, for $RbCaF_3$ in the perovskite structure.

From Fig. 11 two things are apparent: (a) Above $\sim$1350 K the phonon and static pressure curves have no intersection; this implies[8–10] that 1350 K is the melting temperature. (b) The lattice parameter does not exceed the value for which the double well in U-versus-δ curves disappears until $T \gtrsim 1280$ K.

For comparison, the measured melting temperature[19] is 1383 K. Such good agreement between the measured and calculated melting temperatures is partly accidental, due to the neglect of anharmonic corrections. If the potential were perfectly accurate, then the thermal expansion would be accurately predicted at low temperature and the neglect of anharmonic corrections at high temperature would produce a too low theoretical melting temperature by (from an analogy with trends in the alkali-halide results[8]) about 20%. As it happens, however, the present theory for $RbCaF_3$ gives a too low value for thermal expansion at low temperatures (by $\sim$17%) and consequently the predicted melting temperature is only 2% too low.

Similar calculations made using approximations (1) and (2) for the unstable modes show very little difference in the results. For example, values for the room-temperature lattice constant are 4.3927 and 4.3945 Å, respectively, for approximations (2) and (3). The results for thermal expansion and melting temperature using the three approximations are also nearly identical. This neither proves nor disproves the assumptions of approximation (3): What it does show, is that the difference between making a plausible allowance for the unstable modes, and simply discarding them is negligible; principally because they constitute only 2.7% of the total. This would appear to validate discarding the unstable T_2 modes in our studies of the thermodynamic stability of the low-temperature phase.

V. CONCLUSIONS

We have presented a first-principles study of the equation of state and stability of the fluoperovskite, $RbCaF_3$, using the Gordon-Kim approach to derive the interionic potentials and an extended quasiharmonic treatment of the free energy. Our results explain *why* the measured displacive phase transition in this material occurs. The explanation does not involve any subtle anharmonic or polarization effects: The phenomenon is predicted, *ab initio,* within the rigid-ion pair-potential approximation. The reason the system prefers the lower symmetry structure at low temperatures is simply that it allows a more efficient packing of the ions, given the particular pair potentials involved. This aspect of our work (Sec. II) involved relatively simple static energy calculations. With regard to dynamic effects, our most important finding is the demonstration that the *mechanical* instability of the perovskite phase occurs at a temperature an order of magnitude greater than the temperature below which the distorted low-temperature phase becomes stable. We have thus provided rigorous proof of the hypothesis advanced by a number of authors[20–22] that, over a range of temperature, in the perovskite phase the "ideal" locations of the CaF_6 octahedra are, in fact, metastable. What is surprising about our results is the extent of this temperature range ($\sim$1000 K). Our calculations, made in the context of approximation (3) for the free energy, also demonstrate that interplanar correlations between the rotations of CaF_6 octahedra in planes perpendicular to the preferred axis are significantly weaker than intraplanar correlations. This again provides quantitative confirmation of a qualitative hypothesis made by earlier workers.[20,21].

One particular aspect of our approach which should be stressed is that it is the reverse of that usually adopted when discussing structural phase transitions. In the conventional approaches, which derive from the Cochran[23] "soft-mode" theory and Landau's phenomenological free-energy expansion,[24] such transitions are regarded as arising from the "condensation," or "freezing-in," of some symmetry-breaking distortion associated with a soft mode in the high-temperature *higher*-symmetry phase. In our approach the transition can clearly be seen to be dictated by the "unfreezing" of the distortion which produces the *lower*-symmetry low-temperature phase. The structure then transforms to a state which, on average, has the cubic perovskite structure. However, it would appear that there must be some dynamical disorder, involving correlated thermally activated rotations, between the double minima in the lattice potential. Our studies would appear to support the idea[21] that these will be strongly correlated within planes and weakly correlated between planes.

As the temperature is raised the mean fluorine positions move ever closer to their "ideal" locations and their thermal motion will be described more and more accurately by anharmonic vibrations about those locations. As this happens an external probe (e.g., neutron scattering) will see damped plane wave normal modes; i.e., phonons with definite wave vector but finite lifetime. This situation will be achieved much below 1280 K: Specifically, at 300 K the well depth is $\sim\frac{1}{2}kT$ and one should probably expect a damped oscillator response in such circumstances. However, it should be stressed that there is no sharp demarcation temperature between "damped-oscillator" and "double-well hopping" responses. Above 1280 K, there are no unstable harmonic frequencies; but, we predict shortly thereafter ($\sim$1350 K), the crystal melts as the "vibrational pressure" overwhelms the static attraction.

As the temperature is lowered from 1280 K the basic origin of the transition to the low-temperature structure is the lattice contraction, which in fact produces the double well in the potential-energy surface. Further, lowering the temperature simultaneously (a) deepens the double well, through volume contraction, and (b) reduces the mean kinetic energy, thus producing a stronger tendency for the system to lock in to one or the other of the double-well minima. Both of these factors have a critical influence on the transition temperature.

In the low-temperature phase the present theory does appear to predict that soft-mode behavior should be observed. However, one should remember that intrinsic anharmonicity (intermode coupling) must be present and will produce both finite phonon lifetimes and some effect on the transition temperature. Interestingly, for those alkali halides for which the present approach best describes the static energy, the quasiharmonic melting temperature is too low (see discussion above). A similar effect in the present case would improve the agreement between theory and experiment.

These various features of the present approach can be summarized by saying that there is a natural "asymmetry" of the transition, depending on whether it is approached from above or below. We believe that this is a genuine effect, inherent in the form of the static energy, and not an artifact of the quasiharmonic approximation. It is tempting to speculate as to whether or not similar effects may be present for other structural transformations.

A much less speculative conclusion can be drawn: The present work provides an obvious explanation for the observation by Samara *et al.*[25] that the transition temperatures of almost all known zone-boundary instabilities are raised by hydrostatic stress. That this should be the case for $RbCaF_3$ is obvious from the plots of U versus δ for different b values in Fig. 4. One can see that reducing b (i.e., applying hydrostatic stress) *increases* the depth of the double well. It im-

mediately follows that application of the present theory to the compressed lattice would yield a higher transition temperature. However, this qualitative behavior is likely to be present for the rotations associated with *any* zone boundary instability in *any* perovskite structure. Thus all such instabilities should have their transition temperatures raised by hydrostatic stress. This conclusion thus applies to the large majority of all known zone-boundary instabilities. Moreover, in other systems, such instabilities generally involve rotations of molecular units (octahedra, tetrahedra, etc.): If their situation is qualitatively similar to that of the perovskite octahedra, as seems very possible, then the same conclusions may be drawn regarding transition-temperature dependence on hydrostatic stress.

The quantitative results of the present investigation are principally confined to predicting the transition temperature, the melting temperature, and the value and temperature variation of the lattice constant in the perovskite phase (see Table V). We could, in principle, make further quantitative predictions of the temperature variation of f and δ in the low-temperature phase, but these would involve the much more computationally expensive triple minimization of F. However, if one compares f_0 and δ_0, the values that minimize the static energy, with the lowest-temperature experimental values, it can be seen (Table V) that there is very satisfactory agreement: A fact which is further evidence for the reliability of the potentials we used.

The dispersion curves and density of states are also meaningful, if interpreted with caution. Specifically, it should not be expected that the former will provide a fit to the measured dispersion curves comparable with that obtained by other workers[26] who have used rigid-ion models, with ionic charges and short-range forces adjusted to fit the experimental results. In so doing they have absorbed at least some intrinsic anharmonicity into their "harmonic" force constants. Also, one cannot expect a very good fit to the frequencies of polar vibrations. For these, the effects of charge distortion (polarization) must be significant. However, based on experience with the alkali halides,[8] we would argue that frequencies that experience strong polarization effects have a relatively weak volume dependence and therefore do not play a significant role in the determination of the equation of state.

TABLE V. Comparison of various properties of $RbCaF_3$ predicted by the calculation with experimental results.

Property		Expt.	Calc.
Low-temperature structure parameters	$2b$	8.85 Å	8.71 Å[a]
	f	1.0085	1.0090[a]
	δ	0.037	0.034[a]
Room-temperature lattice constant		4.45 Å	4.39 Å
Change in lattice constant from 200 to 300 K		0.18%	0.15%
Displacive transition		193 K	~125 K
Melting temperature		1383 K	1350 K

[a]Obtained by minimization of the *static* lattice energy.

In conclusion, we point out that the application of pair potentials calculated by the Gordon-Kim prescription to equation-of-state calculations for alkali halides,[8,9] alkaline-earth halides,[10] and now, fluoperovskites, has provided a unified picture for the causes of, respectively, melting, superionicity, and displacive-type transitions in these materials. The fact that a single, parameter-free, theory can account for these very different types of phase transitions lends credence to the separate account for each phenomenon. In all cases the phase transition is related to an instability in the lower-temperature phase.

ACKNOWLEDGMENTS

We wish to thank Dr. B. M. Klein, Dr. D. A. Papaconstantopoulos, and Dr. W. E. Pickett for helpful comments on the manuscript. Work at the University of Nebraska was supported by the U.S. Army Research Office under Contract No. DAAG29-80-C-0034.

[1]F. A. Modine, E. Sonder, W. P. Unruh, C. B. Finch, and R. D. Westbrood, Phys. Rev. B 10, 1623 (1974).
[2]M. Rousseau, J. Y. Gesland, J. Julliard, J. Nouet, J. Zarembowitch, and A. Zarembowitch, Phys. Rev. B 12, 1579 (1975).
[3]C. Ridou, M. Rousseau, and A. Freund, J. Phys. (Paris) Lett. 38, L359 (1977).
[4]C. Ridou, M. Rousseau, J. Y. Gesland, J. Nouet, and A. Zarembowitch, Ferroelectrics 12, 199 (1976).
[5]H. Jex, J. Maetz, and M. Müllner, Phys. Rev. B 21, 1209 (1980).
[6]A. Bulou, C. Ridou, M. Rousseau, J. Nouet, and A. W. Hewat, J. Phys. (Paris) 41, 87 (1980).
[7]A. Bulou, J. Nouet, A. W. Hewat, and F. J. Schäfer, Ferroelectrics 25, 375 (1980).
[8]L. L. Boyer, Phys. Rev. Lett. 42, 584 (1979); and Phys. Rev. B 23, 3673 (1981).
[9]L. L. Boyer, in *Proceedings of the 7th International Thermal Expansion Symposium, November 1979* (Plenum, New York, in press).
[10]L. L. Boyer, Phys. Rev. Lett. 45, 1858 (1980); 46, 1172 (1981).

[11]R. G. Gordon and Y. S. Kim, J. Chem. Phys. 56, 3122 (1972).
[12]J. B. Bates, R. W. Major, and F. A. Modine, Solid State Commun. 17, 1347 (1975).
[13]W. A. Kamitakahara and C. A. Rotter, Solid State Commun. 17, 1350 (1975).
[14]S. Green and R. G. Gordon (unpublished).
[15]R. A. Cowley, Phys. Rev. 134, A981 (1964).
[16]L. P. Bouckaert, R. Smoluchowski, and E. Wigner, Phys. Rev. 50, 58 (1936).
[17]L. L. Boyer, Phys. Rev. B 19, 2824 (1979).
[18]G. Lehmann and M. Taut, Phys. Status Solidi 54, 469 (1972).
[19]The measured melting temperature is quoted in Ref. 1 citing Oak Ridge National Laboratory Report No. 2548 (unpublished).
[20]M. Rousseau, J. Phys. (Paris) Lett. 40, L439 (1979); and Ph.D. thesis (Le Mans University, 1977) (unpublished).
[21]M. Rousseau, A. Bulou, C. Ridou, and A. W. Hewat, Ferroelectrics 25, 447 (1980).
[22]A. D. Bruce, K. A. Müller, and W. Berlinger, Phys. Rev. Lett. 42, 185 (1979).
[23]W. Cochran, Adv. Phys. 9, 387 (1960); 10, 401 (1961).
[24]L. D. Landau and E. M. Lifshitz, *Statistical Physics* (Pergamon, London, 1958).
[25]G. A. Samara, T. Sakudo, and K. Yoshimitsu, Phys. Rev. Lett. 35, 1767 (1975).
[26]M. Rousseau, J. Nouet, and R. Almirac, J. Phys. (Paris) 38, 1423 (1977).